Radiative Impacts on the Growth of a Population of Drops within Simulated Summertime Arctic Stratus

JERRY Y. HARRINGTON

Geophysical Institute, University of Alaska, Fairbanks, Alaska

GRAHAM FEINGOLD

Cooperative Institute for Research in the Atmosphere, Colorado State University, Fort Collins, Colorado, and NOAA/Environmental Technology Laboratory, Boulder, Colorado

WILLIAM R. COTTON

Department of Atmospheric Science, Colorado State University, Fort Collins, Colorado

(Manuscript received 19 March 1998, in final form 12 May 1999)

ABSTRACT

The impact of solar heating and infrared cooling on the growth of a population of drops is studied with two numerical modeling frameworks. An eddy-resolving model (ERM) simulation of Arctic stratus clouds is used to generate a dataset of 500 parcel trajectories that follow the mean dynamic motions of the simulated cloud. The 500-parcel dataset is used to drive a trajectory ensemble model (TEM) coupled to an explicit microphysical model that includes the radiative term in the vapor growth equation. The second framework is that of the ERM itself.

Results from the TEM show that the production of drizzle-sized drops is strongly dependent upon parcel cloud-top residence time for both radiative- and nonradiative-influenced growth. Drizzle-sized drops can be produced between 20 and 50 min earlier through the inclusion of the radiative term, which corroborates earlier results. The radiative effect may also cause drops with $r < 10$ μm to evaporate, producing a bimodal size spectrum. Parcel cloud-top residence times as short as 12 min can initiate this bimodal spectrum. TEM results show that the radiative effect increases drizzle drop mass predominately in parcels that tend to contribute to drizzle even in the absence of the radiative term. Activation of large cloud condensation nuclei appears to have a larger effect on drizzle production than does the radiative term. ERM simulations show a weak overall influence of the radiative term. Drizzle onset occurs earlier when the radiative term is included (about 20 min), but there is no strong change in the overall structure or evolution of the cloud.

1. Introduction

The effect of longwave cooling on the growth of water droplets has been postulated to be an important mechanism for the production of large droplets capable of initiating the collision–coalescence process within stratiform clouds and fog layers (Roach 1976; Barkstrom 1978; Austin et al. 1995). Net radiative cooling of the droplets, which is felt predominately at the tops of clouds, allows the latent heat generated during condensation to be dissipated more rapidly than through standard diffusion, thus enhancing condensation rates. If such enhanced condensation can increase the production rate of droplets with radii greater than about 20-μm radius, then there is a potential for enhancing drop collection and precipitation formation (e.g., Cotton and Anthes 1989; Pruppacher and Klett 1997).

While this topic has generated some interest in the microphysics community, the process has yet to be included in detailed microphysical modeling situations with a thorough discussion of the attendant physics. Fuchs (1959) appears to have been the first to discuss the radiative term in the vapor growth equations; however, in his short discussion both the drop and its local environment are considered to be radiating as blackbodies. Since the temperature differences between the drop and the environment are not large, Fuchs showed that the effect can be neglected when considering growth from the vapor. This treatment, however, ignored the fact that droplets at cloud boundaries may gain or lose significant radiant energy through large differentials in the incident fluxes. Early works have considered this

Corresponding author address: Jerry Y. Harrington, Geophysical Institute, University of Alaska, Fairbanks, AK, 99775-7320.
E-mail: jerry.harrington@gi.alaska.edu

effect on the heat budget of an isolated drop existing at cloud top (Roach 1976; Barkstrom 1978). These studies showed that not only is condensation enhanced, but that larger droplets (20 μm radius and greater) can grow through radiative cooling in classically subsaturated environments. Since the radiative effect on condensation is greater for bigger droplets, one would expect to see a differential effect on a population of droplets. This result was briefly discussed in a paper by Guzzi and Rizzi (1980), in which it was shown that longwave cooling allowed large drops to grow while suppressing the growth of smaller droplets (collision–coalescence was not addressed).

More recently, Austin et al. (1995) considered the radiative cooling effect in a mixed-layer model of stratocumulus clouds that included the effects of collision–coalescence on the evolution of the drop spectrum. While the results for the growth of individual droplets substantiated earlier results, collision–coalescence was shown to produce significant numbers of droplets with $r > 25$ μm with currently accepted collection kernels. Their results illustrated that the time required for the onset of precipitation may be reduced by as much as a factor of 4. These results were, however, obtained from a simplified model with a specified population of droplets existing at cloud top and longwave cooling parameterized by the simplified function given in Roach (1976).

The inclusion of the radiative effect into coupled microphysical–dynamical models has been confined to 1D models of stratocumulus and fog. All results have shown that significant production of large droplets occurs within a reasonable time. Bott et al. (1990) included the radiative term in a 1D fog model and showed that it had a differential impact on the drop distribution function with larger drops growing faster than smaller drops. In addition, their results showed that observed oscillations in fog liquid water content (LWC) can be attributed to the radiative effect on drop growth. Ackerman et al. (1995) utilized the radiative effect in an explicit (size-resolving) microphysical framework coupled to a 1D stratocumulus model. Their results showed that cloud-top LWCs, supersaturations, optical depth, and longwave cooling from cloud top were reduced over simulations that neglected the radiative term. An inherent weakness in these 1D models is that they do not explicitly resolve the cloud-scale motions that have a strong influence on the cloud supersaturations and, hence, the droplet vapor depositional growth.

Thus, all previous works have considered the radiative impact on drop growth either in simplified frameworks (i.e., drops residing at cloud top) or in simplified coupled, 1D, microphysical–dynamical settings. In addition, all studies (except Ackerman et al. 1995) have excluded the effects of shortwave radiation on the problem. The above discussion suggests that a gap exists in the link between understanding the radiative vapor growth phenomenon in simplified frameworks and the inclusion of the process in coupled numerical models.

In this paper we focus on the effect that radiative transfer has on the growth of small droplets and the production of drizzle-sized drops. The effects are examined for simulated Arctic stratus clouds (ASC) using two numerical frameworks. The first framework is that of a Lagrangian parcel model driven with trajectory information derived from an eddy-resolving model (ERM; e.g., Stevens et al. 1996a), which is a 2D version of a large eddy simulation (LES) model. This allows us to elucidate some of the processes that may be obscured in a full simulation with an ERM. Rather than simulate a single-parcel trajectory through the cloud, an ensemble of trajectories is derived from the ERM simulation, thus providing a much more representative treatment. The trajectory ensemble model (TEM) is discussed in some detail in Stevens et al. (1996a). The TEM is not meant as a surrogate for simulations of real clouds; rather, its value lies in its ability to accurately address microphysical effects on realistic cloud timescales and paths (an advantage over simpler frameworks) without the attendant difficulties related to cloud dynamic feedbacks. The second framework is that of a full simulation within the ERM itself, the focus being on the production of drizzle in the ERM.

This paper is organized in the following manner. In the first section, we discuss how the radiative information is coupled to the microphysical vapor growth equations. The results from a simulation of ASC with an ERM are discussed in the next section, along with a discussion of the TEM method. Two parcels from the ensemble of parcels are then used to examine the radiative effect on the vapor growth of a distribution of droplets along with how collection, shortwave (SW) radiation, and activation of aerosols affect the results. Once an understanding of the results for single parcels is obtained, results from simulations with the entire ensemble of parcels are presented. The final section includes a set of simulations from the ERM and a discussion of the radiation vapor growth effects on the cloud properties.

2. Radiative and microphysical connections

The microphysical growth of droplets is usually discussed in terms of solutions to a coupled set of ordinary differential equations that describe a balance between the condensation (evaporation) of water vapor and heat diffusion. Radiative heating (cooling) affects this balance through the heat balance of the drop (Roach 1976):

$$L_c \frac{dm}{dt} - R = 4\pi r K (T_r - T_\infty), \tag{1}$$

where L_c is the latent heat of condensation, m is the mass of the drop, r is the radius of the drop, K is the coefficient of heat diffusion, T_r is the temperature at the surface of the drop, T_∞ is the temperature of the envi-

ronment a large distance from the drop, and R is a term that describes the addition or removal of heat from the drop by radiant energy (units of W). Equation (1) indicates that the balance between condensation, which produces heat, and the dissipation of this heat through diffusion is affected by radiation. In the form of the equation given above, a positive (negative) value of R constitutes radiative cooling (warming) since the net diabatic heating is reduced (increased).

The term for the radiative effect, R, is derived by considering the radiant energy budget of a given droplet. Since R is related to the net energy budget of the drop, Roach (1976) showed that

$$R = \int_{\lambda} 4\pi r^2 Q_a(r, c, \lambda)\left[\pi B(T_d, \lambda) - \frac{1}{2}(F^+ + F^-)\right] d\lambda, \tag{2}$$

where Q_a is the absorption coefficient, λ is the wavelength, c[1] the refractive index, T_d the temperature of the droplet, and B the Planck function. For consistency with the two-stream model (Harrington 1997; Harrington et al. 1999), we use an average value of Q_a for a given spectral band, i, and the above equation becomes

$$R_i = 4\pi r^2 \overline{Q}_{a,i}(\overline{r}_k)F_{d,i}$$

$$F_{d,i} = \left[\pi B_i(T_d) - \frac{1}{2}(F_i^+ + F_i^-)\right], \tag{3}$$

where $\overline{Q}_{a,i}(\overline{r}_k)$ is the absorption coefficient averaged over spectral band i and computed at the mean size of microphysical bin r_k; F_i^+ and F_i^- are the upwelling and downwelling fluxes, respectively, for band i; and $B_i(T_d)$ is the band-integrated Planck function evaluated at the drop temperature. It is noted that when applied to a scheme that predicts two moments in a drop size bin, as will be done here, $\overline{r}_k$ changes with time, as discussed in Tzivion et al. (1989). We have defined $F_{d,i}$ as a radiative ''effect'' that includes all of the flux terms. Utilizing R_i in the heat diffusion equation (1) and the following the nomenclature of Tzivion et al. (1989), one finds for the vapor growth equation,

$$\frac{dm}{dt} = C(P, T)\frac{m^{2/3}}{m^{1/3} + l_0}\left[\eta(t) + \frac{r_s L_c \alpha_c m^{1/3} E_d(m)}{KR_v T^2}\right]$$

$$= \frac{m^{2/3}}{m^{1/3} + l_0} C(P, T)[\eta(t) + J(P, T)m^{1/3}E_d(m)], \tag{4}$$

where $\eta(t)$ is the excess specific humidity $[=r_v - r_s(T)]$, r_s is the saturation mixing ratio, R_v is the gas constant for moist air, l_0 is a length scale representing the gas–kinetic effects (e.g., Clark 1973), and the function $C(P, T)$ is defined in Austin et al. (1995). The other terms in the growth equation are defined as

$$E_d(m) = \sum_i^{N_{\text{bands}}} Q_{a,i}(m)F_{d,i} = E_d(\overline{m}_k)$$

$$= \sum_i^{N_{\text{bands}}} \overline{Q}_{a,i}(\overline{m}_k)F_{d,i}$$

$$\alpha_c = \left[\frac{3}{4\pi\rho_l}\right]^{1/3}, \tag{5}$$

with $\overline{m}_k$ representing the mean mass in a drop size-bin k.

In order to utilize this equation in the explicit microphysical model, we must include the above radiative term in the equation for supersaturation and for the growth of droplets. The equation for the water vapor excess (related to supersaturation) is given by

$$\frac{d\eta}{dt} = D - A(P, T)\frac{dM}{dt}, \tag{6}$$

where the D term represents the increase/decrease in η due to dynamics; and $A(P, T)$ is a function associating the integrated mass growth rate, dM/dt, to the change in η. Adding the equation for dM/dt gives

$$\frac{d\eta(t)}{dt} = D - A(P, T)C(P, T)\eta(t)\int \frac{m^{2/3}}{m^{1/3} + l_0} n(m)\, dm$$

$$- A(P, T)C(P, T)J(P, T)\int \frac{m}{m^{1/3} + l_0} E_d(m)n(m)\, dm$$

$$= D - G\eta(t) - \mathcal{R}. \tag{7}$$

The integrals on the right-hand side of (7) are evaluated as discrete sums over the bins k at $\overline{m}_k$. The radiative term is combined with the dynamic term (since η does not appear in the radiative term) $D' = D - \mathcal{R}$, and the equation for the vapor excess becomes

$$\frac{d\eta(t)}{dt} = D' - G\eta(t). \tag{8}$$

The solution to this equation is straightforward as long as the terms D' and G can be assumed to vary slowly over a time step (in our case 2 s); the solution is then

$$\eta(t) = \left[\eta(t_0) - \frac{D'}{G}\right]e^{-G(t-t_0)} + \frac{D'}{G}. \tag{9}$$

By separating the radiative term ($D' = D - \mathcal{R}$),

$$\eta(t) = \underbrace{\left\{\left[\eta(t_0) - \frac{D}{G}\right]e^{-(G(t-t_0)} + \frac{D}{G}\right\}}_{\text{Standard equation}} - \frac{\mathcal{R}}{G}[1 - e^{-G(t-t_0)}], \tag{10}$$

one sees that the radiative effect on η is to reduce (increase) η more quickly under radiative cooling (heating)

[1] Since we will extensively use the symbols m for drop mass and n for the drop distribution throughout, we adopt the symbol c for the index of refraction of water so as to avoid any confusion.

compared to the standard equation. Drops that reside for a considerable amount of time near cloud top can, therefore, drive the supersaturation to values below zero.

In order to solve the condensation equation, we apply the two-moment technique of Tzivion et al. (1989) as modified by Stevens et al. (1996a), which predicts both mass and number in a bin k. In order to redistribute these parameters following condensation, we need to integrate (4) in time. Note that when the radiative term is not included, this integration is straightforward. With the radiative term included, however, the integral is no longer easily solved since a function of m multiplies the radiative effect, and the equation must be solved iteratively. To simplify this calculation, we follow the method described in Stevens (1996) for the effects of ventilation. The hypothesis is that since mass growth is solved locally for each bin, using a mean value of the radiative term for each bin will produce acceptable accuracy. Upon applying this method to the radiative term, the integration of (4) becomes

$$\begin{aligned}\int_{m_0}^{m_f} \frac{m^{1/3} + l_0}{m^{2/3}}\, dm &= C(P, T) \int_{t_0}^{t_f} \eta(t)\, dt \\ &\quad + \overline{m}_k^{1/3} C(P, T) J(P, T) E_d(\overline{m}_k) \Delta t \\ &= \tau + \tau_k = \tau_r \\ m_f &= \left\{ \left[(m_0^{1/3} + l_0)^2 + \frac{2}{3}\tau_r \right]^{1/2} - l_0 \right\}^3, \quad (11)\end{aligned}$$

where τ is the standard forcing not including the radiative effect and is found by integrating (9) over a time step using D instead of D', τ_k is the bin-dependent radiative forcing term, τ_r is the total effect on the mass in bin k, m_f is the final mass after condensation/evaporation at time t_f, and m_0 is the initial mass of the droplet at time t_0.

In order to examine the accuracy of (11), we solve (4) numerically and then compare the results to (11). The computations use E_d values of 10, 20, and 60 W m^{-2}, a drop radius range of 1.6–500 μm, and a supersaturation range of 0.01%–10%. The results of these calculations showed that errors never exceed 1.5%, illustrating the practicality of the approximation in (11). This approximation is thus included in the explicit microphysical model described in Feingold et al. (1994) and Stevens et al. (1996a).

3. Arctic stratus as a test case

A simulated summertime liquid-phase ASC case is used as the basis for our studies. The sounding used to initialize the model was produced from data taken during the 28 June 1980 ASC of the Arctic Stratus Experiment [see Curry (1986) for further details]. The case consisted of a multiple-layered cloud system with an upper deck that had many of the classic features normally observed in lower-latitude stratocumulus. This case was utilized, in part, because of successful simulations that have been carried out with the ERM (Olsson et al. 1998). In particular, we used the nondrizzling runs from this study to be consistent with the TEM framework (described below).

The ERM is a 2D version of the LES model described in detail in Stevens et al. (1996a) and Feingold et al. (1996a). The model used by Olsson et al. (1998) had a grid spacing of $\Delta x = 60$ m and a vertical spacing of $\Delta z = 45$ m, which was reduced to $\Delta z = 30$ m in cloud and then back to $\Delta z = 45$ m above cloud. The strength of this model lies in its emphasis on both dynamics and microphysics through the coupling of an explicit, warm, microphysical model (Tzivion et al. 1989; Stevens et al. 1996a) with a dynamical model that resolves the large eddies. Thus, cloud and drizzle formation respond to resolved eddy motions: cloud condensation nuclei (CCN) are activated to drops (depending on supersaturation, which is in turn related to updraft, w); drop growth through condensation (evaporation) and stochastic collection is explicitly calculated; and drizzle in-cloud residence depends on the size-dependent fall velocity and local w. Although the 2D ERM does not represent the eddy structure as well as its 3D LES counterpart, it does include the essential interactions between large eddies and cloud microphysical properties and provides a valuable framework for testing hypotheses without enormous computational expense (Stevens et al. 1998). To accommodate the inclusion of radiative effects, the current version of the model couples the optical properties of the droplets to an eight-band (three solar and five infrared) radiative transfer model discussed in Harrington (1997). This two-stream model incorporates gaseous absorption by CO_2, H_2O, and O_3 along with a consistent coupling to the bin microphysical model through optical properties that vary according to the bin size. This last feature allows the optical properties to respond to changes in the drop spectrum.

As in Stevens et al. (1996a), during the course of the ERM simulation, 500 parcels are released at various positions throughout the dynamic layer associated with the ASC. These parcels track the air motions throughout the last 2 h of a 6-h ASC simulation. As the simulation proceeds, kinematic (position, velocity), thermodynamic (pressure, liquid potential temperature θ_l, total water r_t), and radiative flux data ($E_{d,i}$ for each band, i) are recorded for future use. A random sample of 25 of the 500 parcels generated by the ERM simulation is shown in Fig. 1a. Cloud base and cloud top occur near 800 and 1150 m, respectively (Fig. 1b), and are fairly constant throughout the simulation period. This sampling of trajectories also shows a strong decoupling of the cloud and subcloud layers, as shown in Olsson et al. (1998). Most trajectories show a regular cycling through the cloud updrafts and downdrafts with few parcels spending extended periods in the vicinity of cloud top or cloud base. Parcel cloud-top residence time, of course, is important for determining the radiative ef-

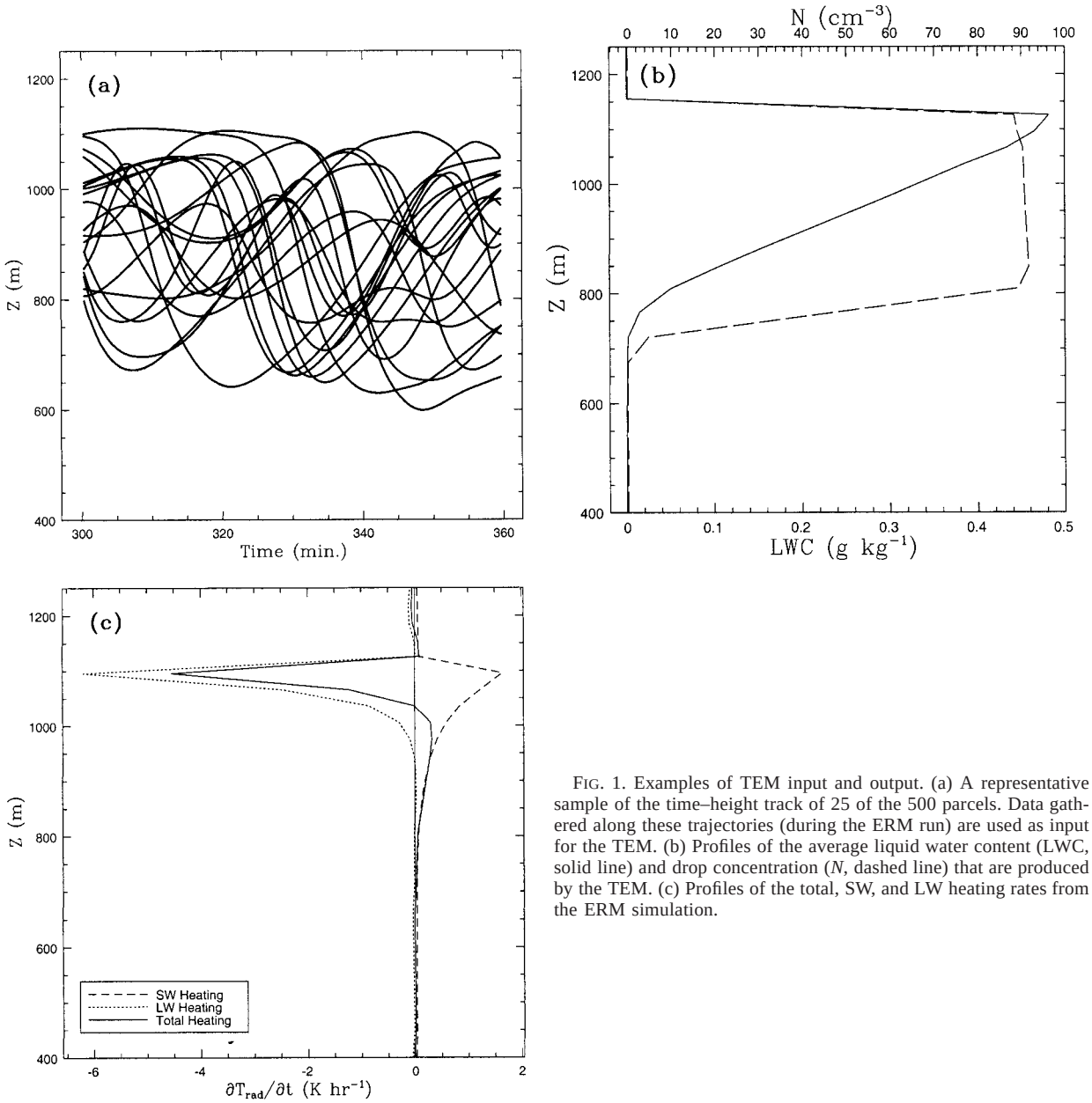

FIG. 1. Examples of TEM input and output. (a) A representative sample of the time–height track of 25 of the 500 parcels. Data gathered along these trajectories (during the ERM run) are used as input for the TEM. (b) Profiles of the average liquid water content (LWC, solid line) and drop concentration (*N*, dashed line) that are produced by the TEM. (c) Profiles of the total, SW, and LW heating rates from the ERM simulation.

fects. At a later stage, the trajectory set is used to drive 500 (or a subset thereof) individual Lagrangian parcel models as part of the TEM.

The Lagrangian parcel model used in the TEM computes the microphysical processes (droplet activation, condensation, and collection) using the same liquid-phase model as in the ERM run. The microphysical model uses 25 bins for which the spacing between bins is determined by mass doubling. The CCN spectrum is assumed to be ammonium bisulphate and follows a log-normal distribution with a median diameter of 0.06×10^{-4} cm and a geometric standard deviation of 2.2. Figure 1b shows an example of the LWC and the drop number concentration (*N*) profiles produced by an ensemble average of all 500 parcels, averaged both temporally and spatially, using the TEM. The TEM reproduces the classic features of radiatively driven stratus; the LWC profile is close to the adiabatic LWC value; and *N* shows a constant-in-height profile, which is characteristic of a cloud with drop activation occurring at cloud base. These profiles compare well with those produced in our ERM studies (see the no-drizzle cases; Olsson et al. 1998).

Figure 1c shows temporally and spatially averaged radiative heating rate profiles produced by the ERM; the fluxes that produce these average profiles are used

as input to the TEM. The strong longwave (LW) radiative cooling at cloud top dominates over the SW heating. Thus, it is expected that the cloud-top region (from about 1000 to 1100 m) will be the preferential location for radiative-enhanced drop growth.

Studying the radiative drop growth phenomenon within the TEM framework has some advantages over studying these effects within the ERM. First, the TEM allows for the examination of microphysical effects without complicating feedbacks associated with dynamics (although this is also a limitation). The TEM also eliminates the spurious spectral broadening associated with advection and diffusion that occur on the ERM's Eulerian grid (e.g., Clark 1974). Since drop growth is simulated on an Eulerian (in mass space) grid, drop distributions are still subject to some diffusive broadening (Clark 1974); however, the top-hat condensation method of Stevens et al. (1996a) mitigates this somewhat. The TEM method, however, also has its disadvantages; the most important of which for this study are the following [see Stevens et al. (1996a) and Feingold et al. (1996b) for a full discussion]. The parcels used in the TEM are advected by the mean wind in the ERM; subgrid turbulence is not considered. Subgrid turbulence could lead to altered cloud-top residence times that may affect the results. Since mixing across interfacial boundaries is not well represented, effects near cloud top may not be accurately represented (although this is also a problem in the ERM). In particular, Stevens et al. (1996a) showed that TEM may also suffer from spurious cloud-top supersaturation production, as in the ERM. There is no mixing between parcels in the TEM, unlike in the ERM, which limits the validity of these results. In addition, the TEM cannot, of course, describe the drizzle process since all drops follow the parcels. This limitation causes a positive feedback that will artificially enhance the drizzle mode. In addition, in a true drizzling cloud, sedimentation causes a reduction in LWC that is not captured by the TEM. Because of these limitations, we refer to drizzle in the TEM framework as ''potential drizzle'' in order to reduce confusion with drizzle production in coupled microphysics–dynamics cloud simulations. Finally, since the radiative fluxes are prescribed along the trajectory, they cannot vary as the drop distribution changes (although the amount of absorption can). These limitations should be borne in mind throughout the subsequent discussion.

Activation of droplets takes two possible forms. In all cases, the total number of CCN available (N_{ccn}) is 100 cm^{-3}. The first method is what we will term ''single-bin activation''; in this scheme all of the activated drops are placed within the first bin of the explicit drop representation (radius of 1.56 μm). This places an upper limit on the time required for the radiative-enhanced growth process to act since activated drops have the smallest possible size. The second method, termed ''distribution activation,'' activates the droplets in accord with a prescribed gamma distribution function ($\nu = 2$ and $D_n = 3$ μm; see Walko et al. 1995). This distribution function is chosen to represent activation from a CCN spectrum with a relative abundance of small particles and a small number of 10-μm radius drops.

The distribution functions produced by the microphysical model will be discussed in terms of the total number and mass of droplets with $r > 20$ μm, and the ''predominant'' radius, r_p, defined by Berry and Reinhardt (1974) as

$$r_p = \left[\frac{3}{4\pi\rho_l}\right]^{1/3} \left\{\frac{\int_0^\infty m^2 n(m)\, dm}{\int_0^\infty mn(m)\, dm}\right\}^{1/3}. \qquad (12)$$

This definition strongly weights the drops with the greatest mass; thus r_p is highly sensitive to changes in the concentration of drizzle-sized drops. For example, Austin et al. (1995) found that $r_p > 45$ μm corresponds to drizzle rates greater than 1 mm h^{-1} in First International Satellite Cloud Climatology Project Regional Experiment clouds. Since drops with radii greater than 20 μm have significant collision–coalescence efficiencies, we use this size to delineate between larger drops (drizzle) and smaller drops (cloud drops).

4. Trajectory parcel model results: Single parcels

In this section we examine how radiation affects the growth of droplets by condensation and collection for a single parcel. Microphysical computations are performed for only 1 h, since beyond this time large numbers of drizzle-sized droplets are produced and the potential sedimentation renders the results of the parcel model invalid. First, we pick a single parcel that follows cloud top (loosely defined as the layer over which radiative cooling is occurring; see Fig. 1c) for the better part of the first hour of the ERM simulation, so that it is exposed to strong radiative cooling. This parcel had the longest cloud-top transect of any parcel in the trajectory set and should in no way be seen as typical. Second, we present results for another parcel that cycles through cloud updrafts and downdrafts and has a more characteristic evolution. A plot of the percent of trajectories that spend a certain amount of time at cloud top (out of 1 h of simulation) shows that few parcels spend more than 30 min near cloud top (Fig. 2). In fact, 50% of all parcels spend less than 8 min in the vicinity of cloud top.

A list of simulations for the single parcels is given in Table 1. The first four simulations in Table 1 are for the parcel that skims the top of the cloud (T = top). The control simulation, TAP (top, all physics), includes all relevant physics with activated drops placed in the first drop bin. A similar simulation, TNR (not shown in the table), which computes condensation without the radiative effect, is used as a basis of comparison with

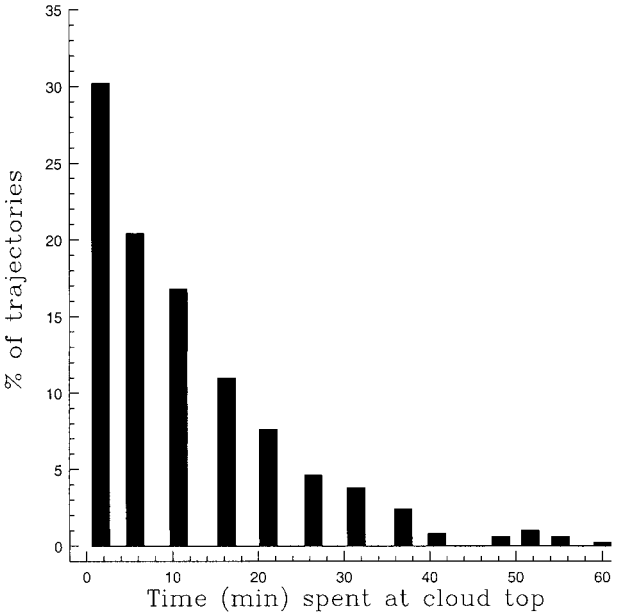

FIG. 2. Histogram of time spent at cloud top for a percentage of the total number of trajectories.

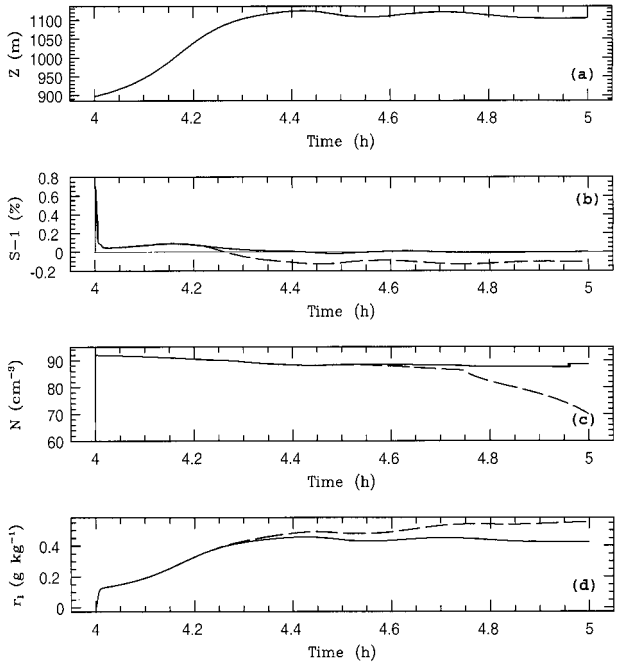

FIG. 3. Time series of the microphysical results for the control runs. (a) The vertical location, Z, (b) supersaturation ($S - 1$), (c) concentration of drops (N), and (d) water mixing ratio r_L are shown for the case without radiation (TNR, solid line) and with radiation (TAP, dashed line).

TAP. Together, these are considered the ''control simulations.'' Sensitivities based on the control case, TAP, that exclude shortwave radiation (NS) or collection (NC) illustrate the magnitude of these effects. The importance of drop activation (either distribution or single-bin) is explored by activating drops conforming to a gamma function (TDA). The last two simulations in Table 1 are for the parcel that cycles through the cloud (C = cyclic). We examine only no-radiation (CNR), radiation (CAP), and distribution activation (CDA) simulations.

a. Control simulations

1) CLOUD-TOP PARCEL: TAP

Time series of the general microphysical results from the control runs (TAP and TNR) are shown in Fig. 3. The parcel's position with height shows that, once initiated, it reaches cloud top within 20 min and remains there throughout the rest of the hour. The mixing ratio (r_l) of the parcel increases continuously as the parcel is advected upward in a supersaturated updraft. Once at cloud top, the parcel without the radiative term maintains a relatively constant mixing ratio (around 0.4 g kg^{-1}); this is consistent with the cloud-top values produced by the ERM. Number concentrations are near 90 cm^{-3} with a slight decrease in time due to collection. Supersaturations oscillate around $S - 1 = 0$ because condensed water remains in the parcel and, since the dynamics are weak ($w \sim 0$), supersaturations cannot be sustained.

For the case with the radiative term (TAP), r_l increases above that of the standard case and increases slowly for the last 0.42 h of the simulation. Most of this increased mass exists in the $r < 20$ μm range with 10% of the mass contained in the drizzle sizes (not shown). Concentrations are similar to the no-radiation (TNR) run until 4.6 h, when the drop concentration

TABLE 1. Simulations with individual parcels. Simulation TAP: control for cloud-top parcel and includes radiation; TNS: same as TAP but without solar absorption; TNC: same as TAP but without collection; TDA: same as TAP but with distribution activation; CAP: control for cyclic parcel and includes radiation; CDA: same as CAP but with distribution activation.

Simulation	Collection	Shortwave	Single-bin activation	Distribution activation	Parcel
TAP	Yes	Yes	Yes	No	Top
TNS	Yes	No	Yes	No	Top
TNC	No	Yes	Yes	No	Top
TDA	Yes	Yes	No	Yes	Top
CAP	Yes	Yes	Yes	No	Cyclic
CDA	Yes	Yes	No	Yes	Cyclic

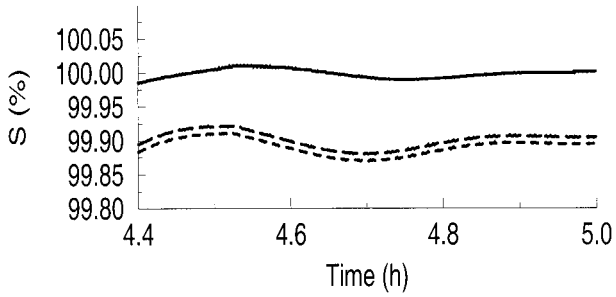

FIG. 4. Time series of the saturation (S) over the last half-hour for the case without the radiative term (TNR, solid line), with the radiative term (TAP, short-dashed line), and for TAP with the Kelvin effect included (long-dashed line).

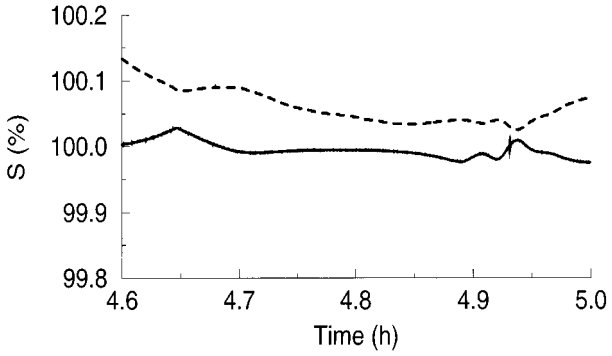

FIG. 5. Time series of the saturation S for TNR (solid line) and TAP (dashed line) when radiative cooling directly reduces θ_l. Results are only plotted over 4.6–5 h in order to focus on the period that is in approximate equilibrium.

begins to decrease because of enhanced collection through the radiative effect. Supersaturations drop below zero and attain equilibrium at a slightly negative value after only a short time at cloud top [see Eq. (9)]. The radiative term, E_d, rapidly increases as the parcel moves toward cloud top, reaching a mean value of about 22 W m^{-2} (not shown), which is within the range given in Austin et al. (1995).

It is interesting to note that our ''equilibrium'' value of $S - 1$ is different from that computed in Austin et al. (1995). In that work, Austin et al. (1995) showed that the inclusion of the radiative term should produce an equilibrium supersaturation that is slightly positive. Our results, however, suggest slightly negative values. As noted by Austin et al. (1995), while the solute term is negligible, the Kelvin (or curvature) term may not be negligible for drops with $r < 5$ μm and, in fact, increases the equilibrium supersaturations. In our derivation of the growth equation, we have ignored this term. In order to test whether or not this term impacts our results strongly, we ran case TAP again except with the Kelvin term included. While this term slightly enhances S (Fig. 4), the effect is quite small (only a 0.05% maximum difference).

The main reason for the subsaturations experienced in our simulations, compared to the supersaturations shown by Austin et al. (1995), is related to the thermal balance that a parcel must attain at cloud top in order to remain there. In Austin et al. (1995), drops are allowed to remain at cloud top and cool radiatively. However, in the ERM, in order for a parcel to remain near cloud top, radiative cooling must be balanced to some extent by entrainment warming.[2] If this is not the case, the parcel would become negatively buoyant and sink through the cloud. To examine a situation similar to that of Austin et al. (1995), simulations TAP and TNR were repeated except that once cloud top is reached, θ_l is reduced by applying the radiative cooling rates for this parcel. (Thus, θ_l does not remain approximately constant as it does in ERM parcel output.) In this case (Fig. 5), the TNR simulation produces S around 100%, while the inclusion of the radiative term produces slight supersaturations similar to those found in Austin et al. (1995). Additionally, we have rederived the equilibrium supersaturation equation of Austin et al. (1995) except that an entrainment-warming term has been added to the analysis. By allowing the radiative cooling and the warming terms to balance one another (which is approximately the case for our cloud-top trajectory) slight subsaturations of about -0.1% are produced. This analysis suggests that the balance between radiative cooling and parcel warming, which must occur if the parcel is to remain at cloud top, is the reason for the slight subsaturations in our case.

The impact of radiation on the drop distribution (dm/dr) is shown in Fig. 6. Note that in the TNR simulation, drop spectra are narrow, whereas in the TAP case, the distribution attains a prominent drizzle mode by 4.8 h, with some large drops being produced after only 0.2 h (12 min) at cloud top (Figs. 6b,c). Note that r_p continually increases as the distribution broadens; however, the 45-μm threshold (Austin et al. 1995) is not reached until after 4.8 h (r_p remains near 10 μm throughout the TNR simulation). Not only does the radiative term produce spectral broadening at the large-drop end, but at the small-drop end as well. The delineation between the large- and small-drop modes is approximately stationary at $r \simeq 10$ μm. It should be noted that the lack of sedimentation will lead to an artificial increase in the number of large drops. However, as will be discussed below, this does not heavily impact the 10-μm delineation for the cloud-drop mode.

The physical differences between the runs with (TAP) and without (TNR) radiation may be understood by examining Fig. 7, which shows τ [proportional to the time-integrated supersaturation; Eq. (11)] for TAP (panel a)

[2] We use the term ''entrainment'' in a fairly loose sense here. Parcels advected in the ERM (for use in the TEM) undergo instantaneous mixing with air above the inversion, causing warming and drying. Since mixing ratios increase above the inversion, drying is minimal in our case.

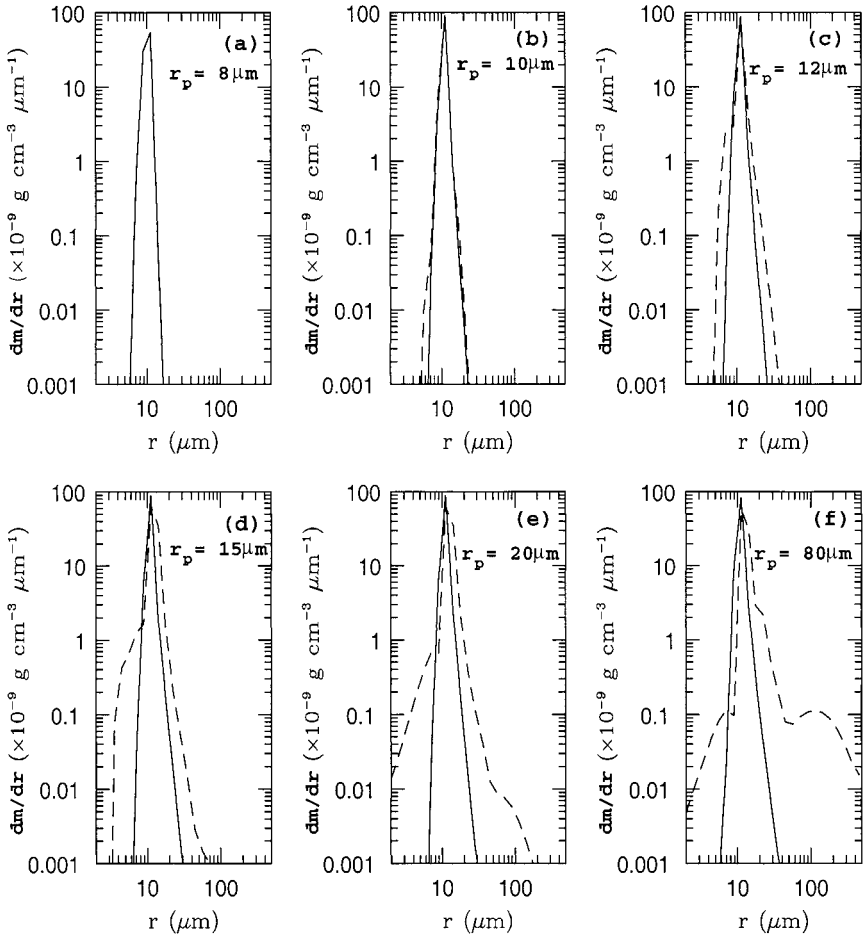

FIG. 6. Plots of dm/dr for selected times during the control run (TAP). For (a) 4.1 h, (b) 4.2 h, (c) 4.4 h, (d) 4.6 h, (e) 4.8 h, and (f) 5.0 h. The dashed line and solid line are for runs with (TAP) and without (TNR) radiation, respectively. Values of r_p are given in the plot.

and TNR (panel b). Cloud drops in TNR and TAP experience similar, initially large, growth rates as supersaturations are produced in updrafts, and once cloud top is reached, τ approaches an equilibrium value. With radiative effects included, droplets with $r > 10$ μm grow rapidly due to radiative cooling at cloud top since the radiative effect, E_d, increases with drop size. The large growth rates near 20 μm show that the production of drizzle-sized drops is significantly enhanced in TAP. Drops with $r > 10$ μm may continue to grow through condensation even in subsaturated environments; thus, after only a short time at cloud top (Fig. 3b), a subsaturated environment is produced. Smaller drops ($r < 10$ μm) do not experience a strong radiative effect (e.g., Guzzi and Rizzi 1980) and thus evaporate in the subsaturated environment. Interestingly, the evaporation of small drops assists the growth of drops with $r > 10$ μm in a fashion akin to the Bergeron–Findeisen process for ice crystals growing at the expense of water drops. This small-mode separation occurs after only about 0.2 h (12 min) at cloud top. The production of the small mode, as will be shown later, is fairly general and occurs near 10 μm because of the rapid decrease in Q_a below this size (e.g., Roach 1976; Stephens 1983). It should be observed that Guzzi and Rizzi (1980) and Bott et al. (1990) noted a differential impact of radiation on distribution growth; however, the production of a small mode was never quantified. It is also interesting that, for the ASC case simulated here, Tsay and Jayaweera (1984) have observed a small-drop mode near cloud top. However, their observations show a delineation near 5 μm, unlike ours that shows up between 8 and 10 μm. Additionally, it is not possible to say what processes produced the observed small mode because of the complicated physics that occur near cloud top. Thus it would be hard to conclude that it is due to a process like that simulated here.

2) CYCLIC PARCEL: CAP

The effects of radiation on drop growth for the cyclic parcel, which is more representative of the ASC, is

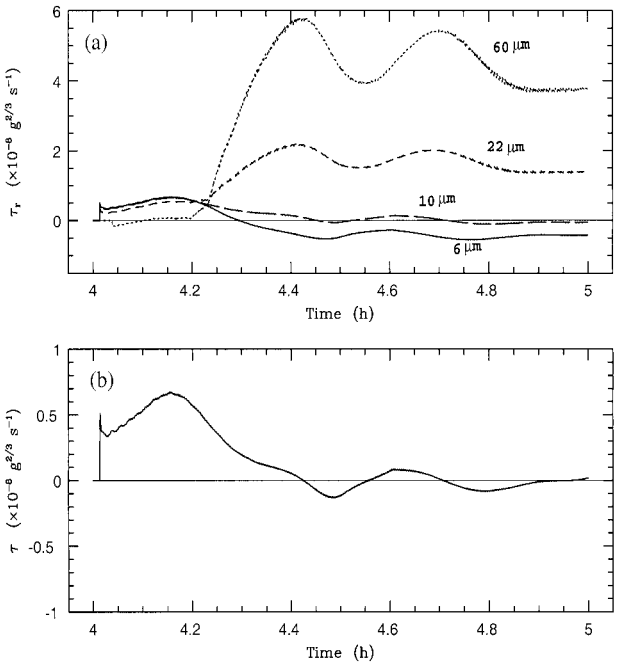

FIG. 7. Time series of τ [Eq. (11)] for control runs. Results including radiation, TAP (a) show τ_r for mean bin sizes labeled in the panel. Results without radiation (TNR) are shown in (b).

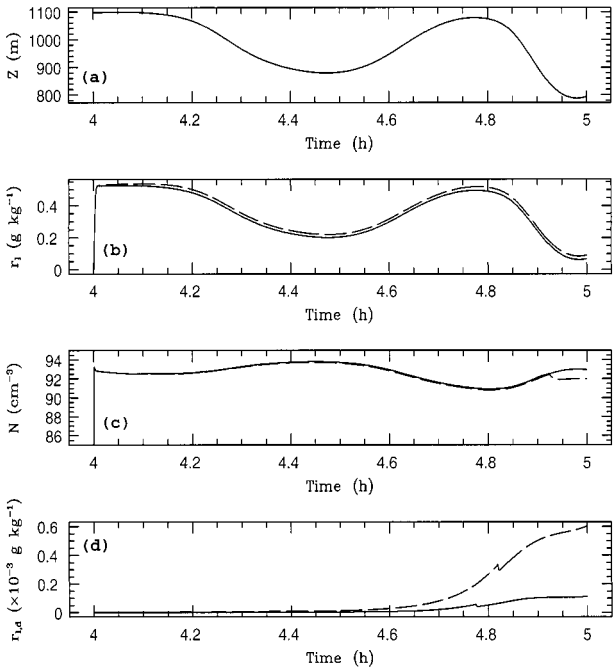

FIG. 8. Time series of the microphysical results for the cyclic parcel. (a) The vertical location Z, (b) liquid water mixing ratio (r_l), (c) concentration of drops (N), and (d) liquid water mixing ratio of drizzle ($r_{l,d}$) are shown for the case without radiation (CNR, solid line) and that with radiation (CAP, dashed line).

shown in Fig. 8. The differences between the radiation (CAP) and no-radiation (CNR) simulations are reduced in this case since the cloud-top residence time of the parcel is much shorter than in TAP. The mixing ratio (r_l) is slightly larger for the radiation case and is generated during the short time that the parcels spend at cloud top. Drop concentrations, N, are only slightly affected by the radiative effects, with a noticeable reduction in concentration occurring toward the end of the simulation. Most of the mass is contained in cloud drops (note the small drizzle drop-mass, $r_{l,d}$) for both the CAP and CNR simulations. The run with radiation, however, is evidently producing enough large droplets through enhanced condensation to initiate greater collision–coalescence rates over the last half hour of the simulation.

b. Results of other sensitivities

In order to examine the importance of various processes on the results discussed above, a set of sensitivity studies is performed (Table 1). To avoid producing a large number of figures, selected information that captures the essence of the sensitivities is presented in Table 2; these include r_p, the fraction of the total mass in drizzle drops (M_f), and concentration tendencies. Instead of r_p itself, we consider the time (t_p) that it takes for r_p to reach 45 μm (Austin et al. 1995). Processes that affect drop concentration are computed as a sum of the processes over the 1-h period;[3] collection (ΔN_{col}), number of drops transferred across $r = 20$ μm (ΔN_{trans}), and number of drops that completely evaporate (ΔN_{evap}) are included in this manner. Intercomparisons among simulations is possible, since approximately the same number of drops are activated in each simulation. Additionally, the results from the control runs (TAP and CAP) and the corresponding no-radiation runs (TNR and CNR) are included as a basis for comparison.

The time required for r_p to reach 45 μm is reduced by about 21 min in TAP and is related to larger ΔN_{trans}, which enhances ΔN_{col} compared to TNR. These times are different from those in Austin et al. (1995), which showed a reduction in t_p from 80 to 20 min due to the radiative effect. In their work, the drops remain at cloud top throughout the computations, warranting comparison with the cloud-top parcel. In addition, their results are produced with initial drop size distributions (dispersions ranging from 0.2 to 0.35), whereas in our case, drops are activated from an assumed CCN size distribution. Concentrations used in Austin et al. (1995) range between 30 and 120 cm^{-3}, which are similar to the concentration used here. Thus, the longer timescales in

[3] For simulations that did not reach $r_p = 45$ μm in 1 h, we ran the simulation for the full 2 h of trajectory data available. Summed processes as referred to above are for the full simulation period.

TABLE 2. Sensitivity results for single parcel: t_p is the time for the distribution to reach $r_p = 45$ μm in minutes; M_f is the fraction of total mass in drizzle drops in %; ΔN_{trans} is the number of drops transferred across $r = 20$ μm; ΔN_{col} is the number of drops collected; and ΔN_{evap} is the total number of drops completely evaporated in cm^{-3} (*** means that $r_p = 45$ μm was never reached during the simulation time).

Simulation	t_p	M_f	ΔN_{trans}	ΔN_{col}	ΔN_{evap}
TNR	69.3	0.039	9.0×10^{-5}	2.39	1.846
TAP	48.0	9.58	0.33	10.94	8.62
TNS	45.0	23.4	0.376	20.14	10.66
TNC	***	0.005	0.17	0.0	8.94
TDA	18.7	83.22	1.77	63.33	8.22
CNR	80.7	0.165	2.5×10^{-9}	2.66	0.138
CAP	72.8	0.67	1.1×10^{-7}	2.89	0.94
CDA	31.3	99.9	0.16	47.9	59.0

our case are likely due to the fact that we do not begin with some large drops already in existence. Additionally, differences in the collection kernels used will add to the differences in the times needed for potential-drizzle production.[4] The cyclic parcel shows weaker effects compared to the cloud-top parcel, with reductions in t_p that are much smaller (only 8 min); this is consistent with the fact that the transfer of drops and collection is only slightly enhanced.

Without shortwave absorption (TNS), drops experience larger cooling rates and, hence, greater condensational growth, which significantly increases M_f but not t_p (potential-drizzle production occurs only 3 min earlier in TNS). This is consistent with the similar transfer rates (ΔN_{trans}) between the cases. The size dependence of SW absorption is responsible for this similarity since drops with $r < 20$ μm absorb less SW radiation than drizzle drops (Stephens 1983). Thus, SW heating does not offset the LW cooling much for cloud drops and, therefore, transfer rates and t_p are not greatly affected. The bigger impact is noticed in M_f and ΔN_{col}, since SW absorption strongly affects the condensational growth of the drizzle drops.

Collision–coalescence, of course, greatly affects the mass partitioning within the drop distribution. Condensation by itself, along with long- and shortwave effects (TNC), never produces a significant drizzle mode. Values of ΔN_{trans}, however, are greater than in TNR, showing that radiatively enhanced condensation significantly affects the initial production of drizzle-sized drops. The complete evaporation of drops (ΔN_{evap}) in TNC is similar to the run with collection (TAP), indicating that drops with $r > 20$ μm are not the predominant cause of the evaporation of drops with $r < 10$ μm. Although drops with $r > 20$ μm might be expected to affect evaporation rates of small droplets (e.g., Fig. 7), their numbers are too small to have a large impact. Thus, *it is the radiatively enhanced condensation of drops in the $r = 10$ to 20 μm range that is the main reason for the evaporation of small cloud drops in the model and, hence, the spectral broadening at small sizes.*

Activating drops in the 1.56–10-μm range (TDA) as opposed to single-bin activation (TAP) has a strong effect on drop growth. The time required for the production of significant drizzle drops is much reduced in TDA. These results are more comparable to Austin et al. (1995) and show the strong effect an initial spectrum has on the results. Cloud-drop transfer and collection rates increase as the few 10-μm drops activated may rapidly grow to $r > 20$ μm. Even though more drizzle drops are produced in TDA, ΔN_{evap} is similar to TAP and TNC, showing a consistent effect on $r < 10$ μm drops in each case.

Sensitivities conducted with the cyclic parcel show little difference between the no-shortwave (CNS) and no-collection (CNC) simulations and, thus, are omitted. The simulation that included the activation of a few large drops (CDA) shows a significant decrease in t_p, similar to the cloud-top parcel results. The decrease in t_p is more pronounced in the CDA simulation than in the corresponding TDA experiment. The results are more dramatic than in the top-tracking parcel experiments because parcels that spend a long time at cloud top are likely to produce drizzle anyway. In the cyclic parcel case, radiative enhancement of vapor growth does not greatly alter the time that it takes to produce large drops. Activating a few large drops in addition to the radiative effects, however, shows a strong impact that reduces the time necessary for drizzle-size drop production. This suggests a result that will be discussed in the ensemble section: *it appears that the radiative effects alone enhance drizzle-sized drop production mostly in parcels that will likely produce drizzle drops anyway.*

5. Trajectory parcel model results: Ensemble results

The results presented in the previous section for the single parcel trajectories, while elucidating the radiative effects on the distribution function, are not representative of the cloud as a whole. Therefore, in this section we examine the effects of radiation on drop growth for an ensemble of cloud trajectories. The TEM is run for all 500 trajectories, and the results are averaged temporally and spatially. The temporal average is computed over a 1-h simulation period in order to find the average effect of radiation on the cloud-drop distribution. Profiles are produced by averaging the results into $\Delta z = 20$ m spacings, which is similar to the spacing used in the ERM. Since temporal and spatial averages do not convey information concerning temporal evolution, results comparing the dependence of various processes on

[4] We used Long's (1974) collection kernel; however, the mass weighting used here gives results similar to Hall's (1980) collection kernel. See Tzivion et al. (1987) for a discussion of the weighting.

the cumulative cloud-top residence time (t_c) are also presented.

Conducted simulations include those shown in Table 1, except that the first letter in each acronym is removed (e.g., TAP is now simply AP). As in the above sections, the total CCN concentration available for nucleation is $N_{ccn} = 100$ cm^{-3}. In order to examine the importance of CCN concentrations, parcel trajectories from an ASC simulation with $N_{ccn} = 500$ cm^{-3} are also used in the TEM. Simulations conducted with the TEM are for no-radiation (500NR) and radiation (500AP) and utilize the same physics as the AP simulation. Results are presented for the AP control simulation first, followed by sections that discuss the various sensitivities.

a. Control simulation (AP): $N_{ccn} = 100$ cm^{-3}

As discussed in section 3, the hour-averaged general microphysical profiles (r_l, N, in Fig. 1b) show that the TEM captures the basic microphysical structure of the ASC with r_l increasing linearly with height and N constant. The major differences between the TEM simulation and an ERM simulation are that drops are not able to sediment and that mixing between parcels does not occur; thus the r_l and N profiles are sharper than they would be in the ERM. This, of course, is a limitation of the results presented in this section. However, one must keep in mind the advantages and goals of using the TEM approach (see section 1).

From the results presented in the last section, one would expect radiative cooling at cloud top (AP) to substantially increase r_l and drizzle drop mass. This is indeed the case (Fig. 9a), as cloud-top mixing ratios are increased by almost 0.1 g kg^{-1}. This is certainly an overestimate since in a real cloud, one would expect cloud top r_l to decrease as large drops undergo sedimentation (cf. Ackerman et al. 1995). The percentage of mass and number concentration (M_f and N_f, respectively) that exists in the drizzle size range ($r > 25$ μm) shows significant enhancement both at cloud top and cloud base in AP. Cloud-top enhancement of drizzle drop mass must be due to collection in NR, while in AP, the radiative effect and collection work in tandem. The cloud-base maximum is due to the complete evaporation of small drops in the subcloud region (below about 750 m). This maximum is enhanced in the AP simulation because of the larger subsaturations below cloud base (not shown).

Potential-drizzle production, as characterized by r_p, is significantly enhanced through radiative effects at cloud top (Figs. 10a,b) with values reaching 25 μm. As parcels continually cycle through the cloud without sedimentation depleting large drops, larger r_p values produced at cloud top cause increases throughout the domain. A secondary maximum in r_p also appears below cloud base in AP, which is due to the evaporation of small cloud drops as discussed above.[5] The cloud-top maximum in both cases is due to collection near cloud top (∂N-∂t_{col}, Fig. 10c), since r_l is greatest within this region. Because the potential production of drizzle drops is related to parcels that spend time at cloud top, this works in unison with the radiative effect. As the results for the AP simulation illustrate, collection rates are significantly increased in the vicinity of cloud top but are similar to NR throughout the lower portions of the cloud.

At cloud top, a comparison of the mass distribution function (dm/dr in Fig. 10b) for the AP and NR simulations shows an increase in spectral breadth with increases in both small- and large-drop concentrations. The 9–10-μm size appears to be a general delineation between drops that continue to grow through radiative effects and those that evaporate in these simulations, since the feature shows up in the ensemble-averaged results. This effect is likely enhanced by the fact that large drops cannot sediment away from the cloud-top region. However, the drops that contribute most to this effect (10–20 μm) have small sedimentation velocities (0.01–0.04 m s^{-1}; Beard 1976) and will fall only about 7 m in 12 min. This, in conjunction with the result from the single parcel showing that only 12 min near cloud top is necessary for smaller drops to evaporate, suggests that this form of broadening is a robust feature.

1) ANALYSIS OF CLOUD-TOP TRAJECTORIES

The above results show that cloud-top trajectories are important for the potential production of drizzle drops; thus the histogram shown in Fig. 2 is illuminating. The histogram is characterized by an exponential-like decay of time spent at cloud top (t_c). Mean time spent within the defined cloud-top region is just under 12 min. Most parcels spend between 2 and 4 min at cloud top, while few parcels spend more than 20 min within this region. From this histogram, it is immediately evident that significant enhancement of drizzle production is dependent upon increasing drizzle growth in the majority of parcels that have shorter cloud-top residence times. Clouds in which only trajectories with the longest cloud-top times contribute to drizzle production should produce little drizzle overall.

In order to quantify which trajectories are likely to contribute to drizzle production in an ASC, we average M_f over each trajectory and plot this as a function of t_c (Fig. 11). Drizzle mass fraction is highly correlated with t_c in both the AP and NR simulations. Indeed, in the NR simulation M_f shows a continuous increase for trajectories with $t_c > 30$ min. The drop in M_f after 55 min is due to two factors: 1) only a few parcels have $t_c >$ 55 min, and some of these spend a fair amount of time

[5] Values of r_p were not computed if $r_l < 0.01$ g kg^{-1}, to eliminate numerical problems.

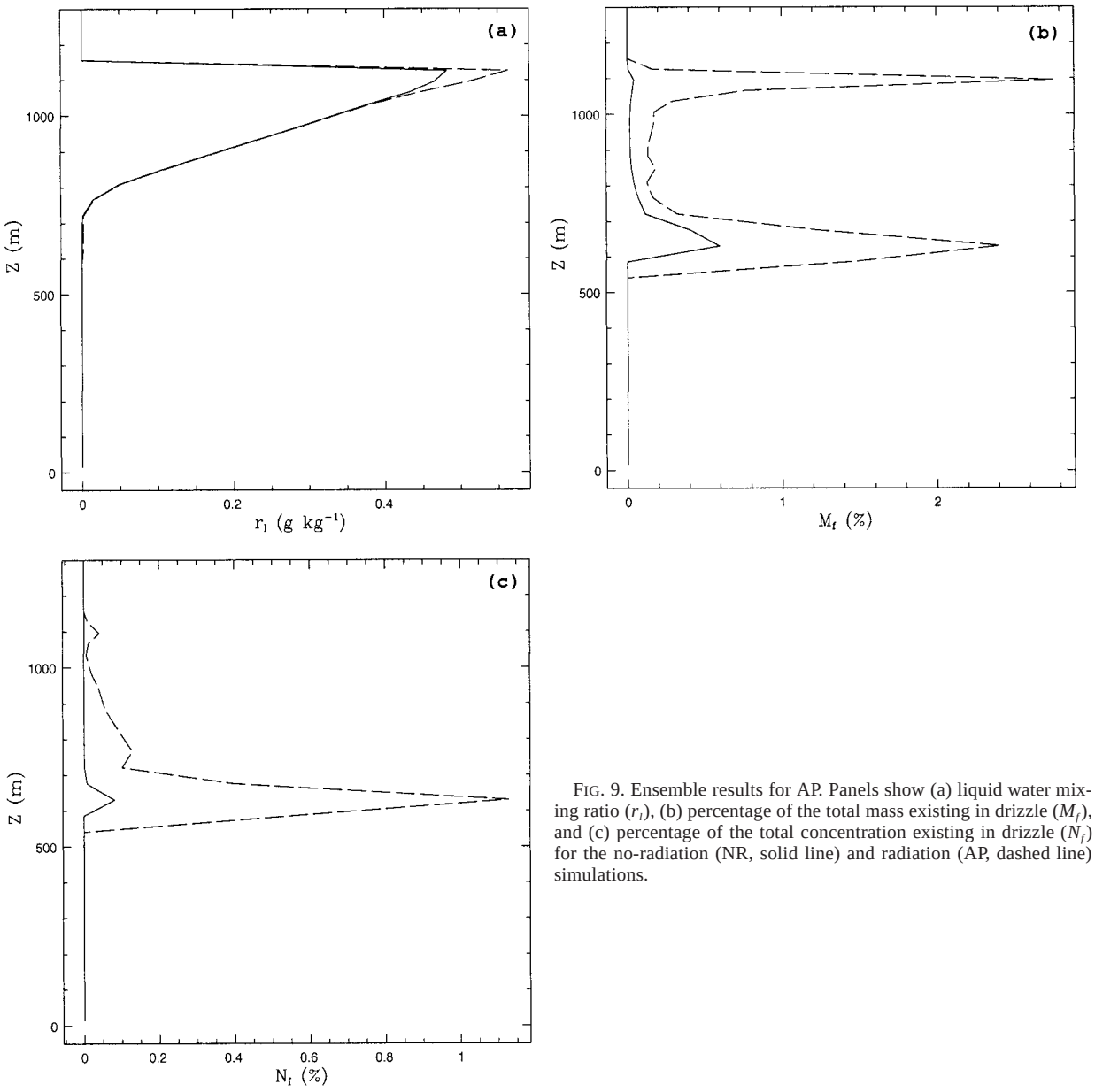

FIG. 9. Ensemble results for AP. Panels show (a) liquid water mixing ratio (r_l), (b) percentage of the total mass existing in drizzle (M_f), and (c) percentage of the total concentration existing in drizzle (N_f) for the no-radiation (NR, solid line) and radiation (AP, dashed line) simulations.

below the radiative cooling maximum, and 2) the 60-min point is zero since no parcels have $t_c = 60$ min. The mass percentage is significantly enhanced in AP through the combination of larger condensation and collection rates. However, as comparison to the inset shows, the same subset of trajectories that contribute to potential drizzle production in NR are affected strongly by the radiative term in AP. Thus, radiation appears to enhance drizzle mass within parcels that potentially contribute to drizzle production anyway. If the radiative effect would increase potential-drizzle production in a broader set of trajectories (i.e., have a strong effect on the more numerous parcels with shorter cloud-top residence times), drizzle potential would be enhanced much more substantially.

b. Sensitivities to control simulation

In order to examine the importance of certain processes in the ensemble simulations, we follow a similar schedule of sensitivity tests as in the TAP simulations discussed in section 3; however, CCN concentration effects are also considered. In these sections we concentrate on physical variables that show the strongest contrasts with the control simulation and, thus, lead to quantitative information about the process. Therefore, we

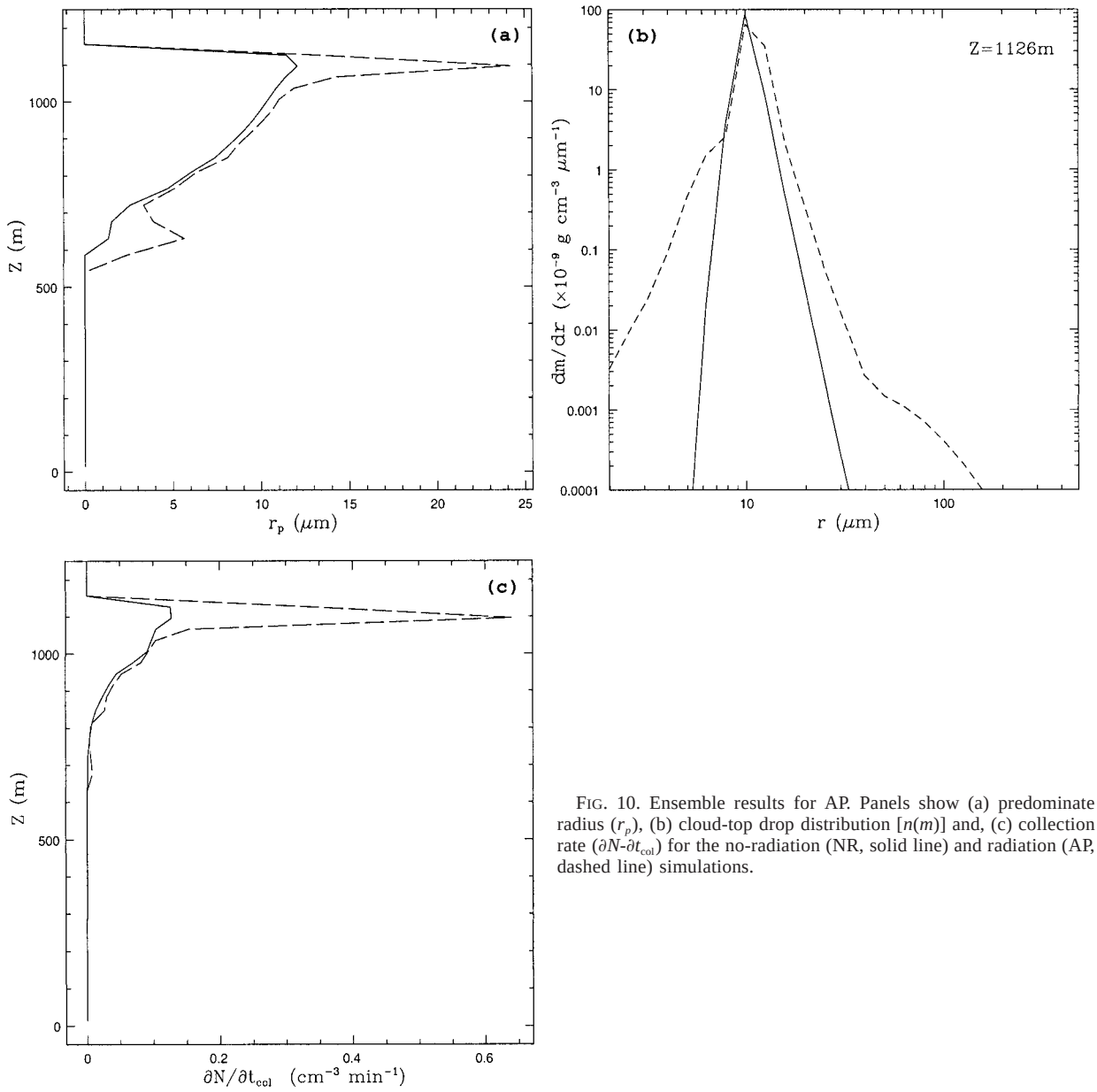

FIG. 10. Ensemble results for AP. Panels show (a) predominate radius (r_p), (b) cloud-top drop distribution [$n(m)$] and, (c) collection rate (∂N-∂t_{col}) for the no-radiation (NR, solid line) and radiation (AP, dashed line) simulations.

concentrate most of our effort on cloud-top residence time plots since these appear to illustrate the effects most strongly. Effort is concentrated on simulations that produce the largest differences with respect to the control.

1) SIMULATION WITH DISTRIBUTION ACTIVATION (DA)

Since activating a few large drops appears to have a significant impact on potential-drizzle production (see section 4), a sensitivity to the control (AP) is run by placing drops in bins up to $r = 10$ μm (as in TDA) with a distribution function that decreases rapidly with radius.

The impact of activating a few large drops (termed simulation DA) is shown in Fig. 12. Increasing the size of the activated drops so that a few 10-μm drops are produced drastically changes the results. Initialized large-drop concentrations are near 2×10^{-1} cm^{-3}, which is higher than the concentrations used by Feingold et al. (1999). Drizzle drop mass is increased throughout the cloud layer (Figs. 12a,b) as reflected by the large increase in M_f and r_p values. The rapid increase in M_f for $t_c > 20$ min shows that significant collection

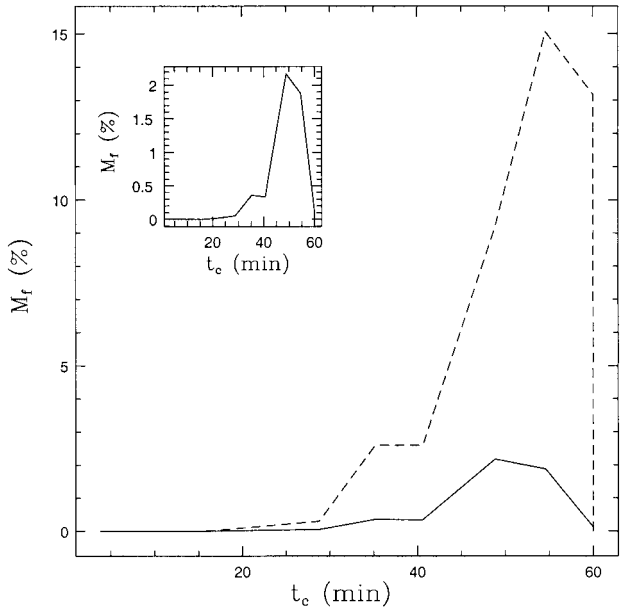

FIG. 11. Ensemble results for AP where t_c is the cloud-top residence time. Plots of drizzle drop mass percentage (M_f) are shown for the no-radiation (NR, solid line) and radiation (AP, dashed line) simulations. The inset in M_f is for NR.

is occurring for parcels with these shorter cloud-top residence times. For the simple activation cases above, radiative effects alone did not significantly enhance potential-drizzle production for a broader set of parcels (i.e., the same subset of parcels contributes to drizzle in AP as in NR). Drizzle enhancement for a broader set of parcels (with t_c less than 30 min) occurs in DA through the combination of large-drop activation and radiative effects. In order to discover how much of this ''broadening'' is due to radiation or to large CCN activation, a second simulation was conducted with DA activation but without radiatively affected growth (DA No-Rad.). Figure 12c shows that the magnitude of M_f is reduced without the radiative effect (as expected); however, notice that increases in M_f still occur for $t_c >$ about 20 min. This result, in conjunction with the AP and NR simulations, seems to suggest that the activation of large CCN may be more effective at producing drizzle than the radiative effect alone.

Together, these results suggest that increased drizzle production in parcels with shorter cloud-top residence times is a function of the size of the activated drops and the CCN concentration. Because increasing the drizzle production in short t_c parcels is important for reducing the time of potential-drizzle onset (see t_p values in Table 2), activating a few large drops in conjunction with enhancement through radiative effects can significantly enhance the potential for drizzle production.

2) SIMULATION WITH $N_{ccn} = 500$ cm^{-3} (AP500)

Increases in drop concentrations are expected to produce less drizzle because the available vapor is distributed over more numerous, and smaller, droplets. In order to examine this effect, the TEM was initialized with trajectories generated from an ASC simulation with 500 cm^{-3} CCN (Olsson et al. 1998). As expected, potential-drizzle production was suppressed, with drizzle-sized drops containing only a small amount of the cloud-water mixing ratio in both the radiation and no-radiation simulations (not shown). The percentage of mass associated with drizzle drops (M_f, Fig. 13) is significant only for parcels with the longest cloud-top residence times (in excess of 50 min). Because few parcels have such long cloud-top traverses (Fig. 2), this enhancement has little effect on the overall TEM cloud structure. The larger M_f for parcels with $t_c \geq 55$ min is due to the production of a few drizzle drops through radiatively enhanced condensation, which rapidly accelerates collection because of the large-drop concentrations and the high mixing ratios at cloud top. A simulation without the radiative effect was also done for the 500-cm^{-3} case, and this produced an insignificant amount of drizzle-size drops over the 60-min period.

6. ERM simulations of ASC with radiation–condensation coupling

In order to illustrate the importance of the radiative term in a fully coupled simulation, a small set of studies has been done with the ERM. The ERM simulations give a more realistic estimate of the impact of the radiative term on the evolution of simulated ASC, because of the feedbacks between dynamics and microphysics. These feedbacks affect the cloud-top residence times of parcels and the condensation and collection algorithms as they are subjected to the numerical effects of advection and diffusion (Stevens et al. 1996a). Simulations with the bin microphysical model are initialized and run for a 6-h time period using 100-cm^{-3} CCN concentrations. Model integrations have been carried out for two pairs of studies. The first consists of a set of simulations both with (RAD) and without (NRAD) the radiative term. The second set of simulations does not include the effects of sedimentation, and again, explores the difference between simulations with and without the radiative term. The model setup is the same as that used in Olsson et al. (1998), the essence of which was given in section 3 above. The above sets of simulations are not intended to be an all-inclusive study but are performed to illustrate the impact of the radiative effect in a fully coupled model. The full impact of the radiative term in ERM and LES will be explored in future work.

Full ERM simulations

Time series of relevant quantities for simulations RAD and NRAD are shown in Fig. 14a. The maximum r_p attained during the simulations is plotted in Fig. 14a. Both RAD and NRAD produce small r_p values throughout the first hour of the simulation (the model spinup

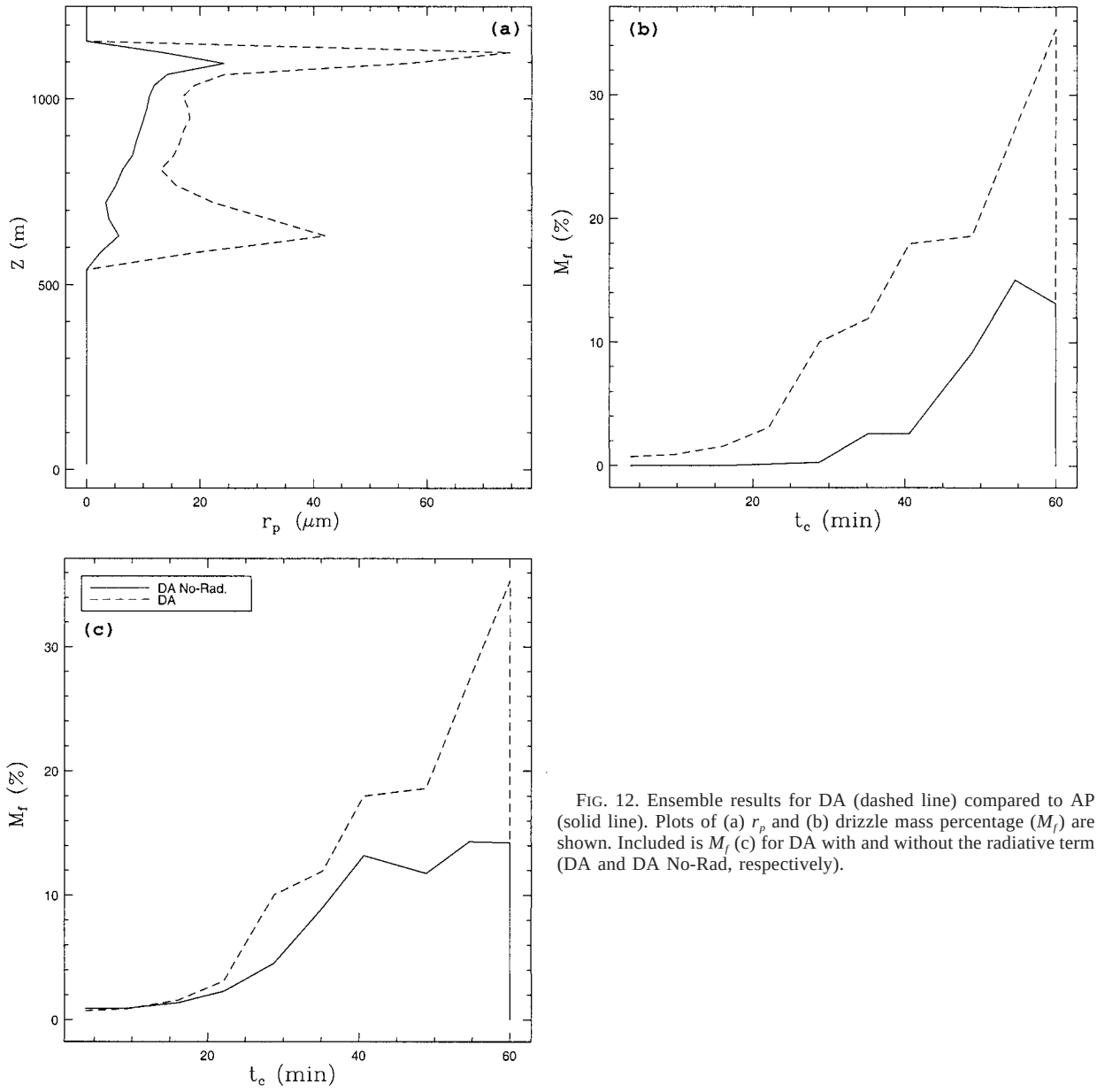

FIG. 12. Ensemble results for DA (dashed line) compared to AP (solid line). Plots of (a) r_p and (b) drizzle mass percentage (M_f) are shown. Included is M_f (c) for DA with and without the radiative term (DA and DA No-Rad, respectively).

period). Maximum values are collocated with cloud top, which is the region of dominant collision–coalescence. The RAD and NRAD time series are similar except that the RAD simulation produces a rapid change in r_p about 20 min earlier. One should keep in mind that the first 2 h of the simulation constitute a spinup period for the ERM dynamics, and therefore one should refrain from drawing conclusions during this period.

The time series of the maximum LWC and liquid water path (LWP) (Figs. 14b,c) shows that, during the rapid period of collision–coalescence growth near 1.75 h, LWC_{max} decreases in RAD compared to NRAD since drops sediment away from cloud top. Additionally LWP_{max} is higher in RAD compared to NRAD because drizzle has not yet reached the surface; thus there is more liquid water distributed throughout each atmospheric column in RAD. The radiative term allows for more condensation at cloud top in RAD, which increases the LWP_{max}; however, the radiative term also increases drop sizes causing larger drizzle fluxes at cloud top and, hence, smaller LWC_{max}. Once a significant number of large drops is produced, the LWPs in RAD also fall below NRAD due to precipitation [similar to the impact shown in Ackerman et al. (1995)]. Even though there is a difference in the time of precipitation onset between RAD and NRAD, these microphysical differences are not great enough to produce a bifurcation in the dynamics. This is illustrated in Fig. 14d, where

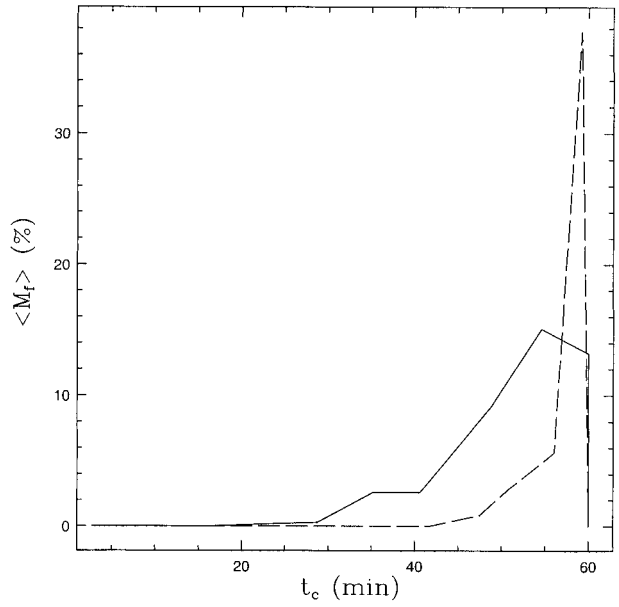

FIG. 13. Plots of drizzle mass percentage (M_f) are shown for AP (solid line) and 500AP (dashed line).

$\overline{w'w'_{\max}}$ in RAD and NRAD are seen to track one another closely.

Both simulations are actively producing drizzle-sized drops by 2 h into the simulations. However, structural differences in the clouds exist at this time as shown by profiles of the drizzle flux[6] (which are averaged over the horizontal domain and over 15-min time intervals) at 2 and 3 h into the simulation (Figs. 15a,b, respectively). This illustrates the more rapid development of precipitation in RAD, which, by 2 h, has developed throughout the cloud layer. It takes the NRAD simulation almost a full hour to produce the same effect (Fig. 15b).

Although these simulations show that the radiative term has some effect on the simulated microphysical evolution of ASC, the effects are not as strong as in the TEM. While there are many differences between the TEM and the ERM, the following are possible reasons for the differences between the results.

1) *Lack of sedimentation in the TEM.* As noted previ-

[6] This flux is defined as $F_{\text{drizzle}} = \Sigma_{i=1}^{25} m_k v_k$, where v_k and m_k are, respectively, the terminal fall speed and water mass in the kth bin.

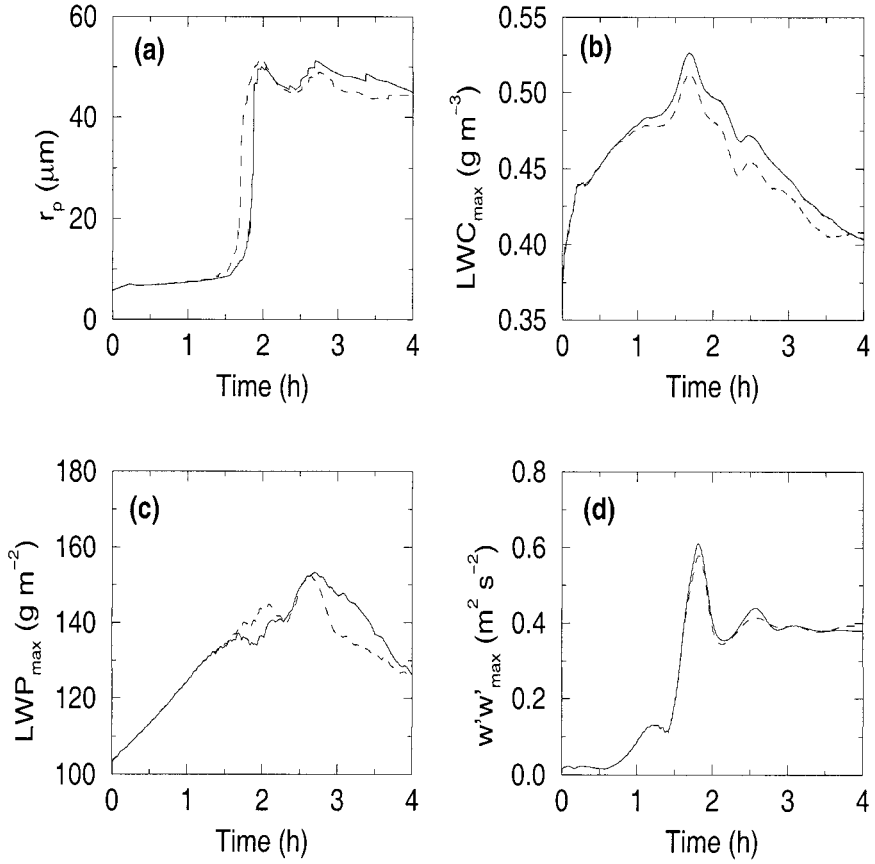

FIG. 14. ERM time series of (a) maximum r_p, (b) $LWC_{\max}$, (c) $LWP_{\max}$, and (d) $w'w'_{\max}$ for NRAD (solid line) and RAD (dashed line).

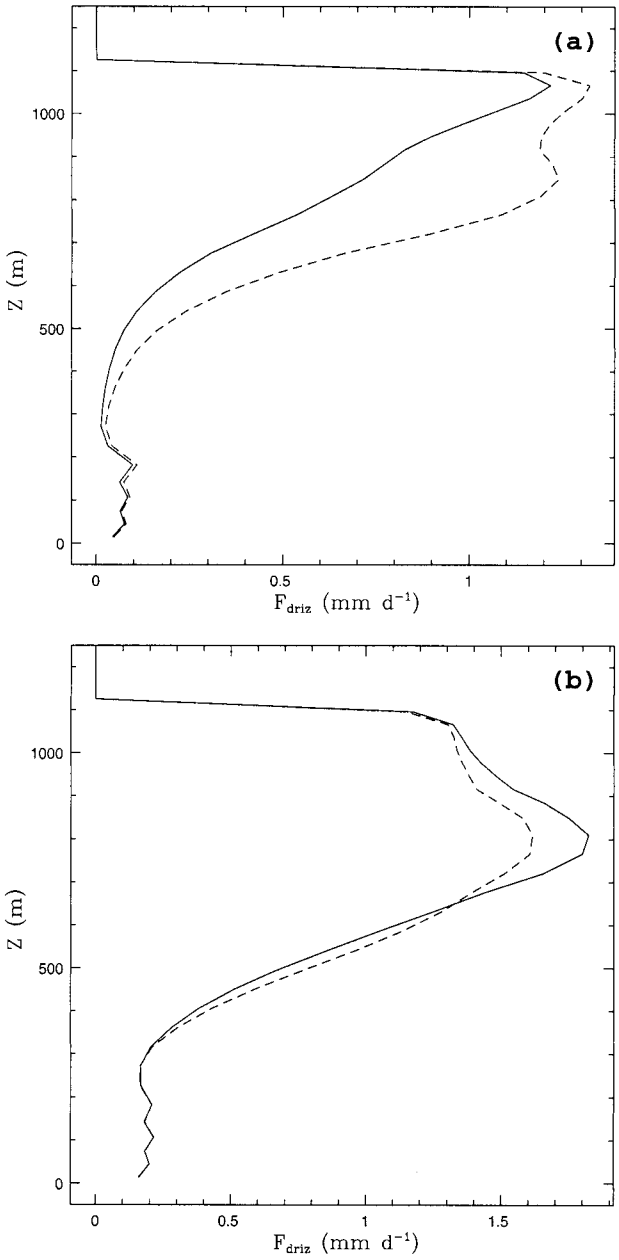

FIG. 15. ERM profiles of the drizzle flux (F_{driz}) at (a) 2 h and (b) 3 h.

ously, the lack of sedimentation in the TEM produces an artificial positive feedback in the production of large drops and is a possible cause of the differences between the TEM and ERM results. Simulations with the ERM in which sedimentation is disabled show that there is only a small difference between the radiation and no-radiation cases (not shown). Therefore, it appears that the lack of sedimentation in the TEM is not the main reason for the differences.

2) *Lack of mixing between parcels in the TEM.* Since parcels in the TEM are considered closed—that is, they do not mix with one another—the TEM represents only grid-resolved advection along each trajectory. This could have some bearing on the differences between the TEM and ERM results. For example, if drop spectra at cloud top that are experiencing rapid broadening were able to mix with spectra lower down in the cloud where broadening is minimal, this would diminish the radiative impact in the cloud-top parcel and increase it in parcels lower down. However, because only a small fraction of parcels spend significant periods of time at cloud top, their ability to mix with other parcels would likely diminish the overall effect. The degree to which this would be true would be determined by the representation of the mixing process. The concept of interparcel mixing is being explored in our current work but is beyond the scope of this study.
3) *Spurious broadening.* Advection in Eulerian space suffers from some degree of numerical diffusion, and explicit microphysical models (such as those used in both the TEM and ERM) experience some spurious spectral broadening as a result of this (e.g., Clark 1974). In the TEM, droplets grow along a trajectory derived from the Eulerian advection but, nevertheless, do not experience any spurious broadening (other than that associated with the bin microphysics) because advection of material substance (drops) from adjacent areas is not represented. The extent of this numerical broadening, relative to the broadening associated with the radiative term, needs to be explored.
4) *Spurious supersaturation production at cloud top in the ERM and TEM.* Generally, both TEM and ERM simulations may produce spurious maxima in supersaturation near cloud top (Stevens et al. 1996b). However, computations of both mean and updraft-averaged supersaturations in the TEM (S_u, Fig. 16) show a very weak maximum near cloud top and, therefore, small spurious drop growth rates. This is not the case in the ERM where both S_u and the mass growth rate in updrafts (dr_l/dt) show a significant maximum near cloud top (Fig. 16). While these results are suggestive, the amount of *time* that a given drop experiences the maximum in S is unknown; hence it is rather unclear whether or not this effect biases the ERM results. But because the secondary maximum in S occurs in the same region that the the radiative effect is strongest, this could diminish the overall impact of the radiative effect in the ERM.
5) *Differences in initialization.* Finally, within the TEM framework, drops are activated in an environment that has dynamics that are already spun up. In contrast, the drizzle process is initiated in the ERM during the period of time when the model dynamics are spinning up. As such, the drops in the ERM are subjected to a different history than those in the TEM.

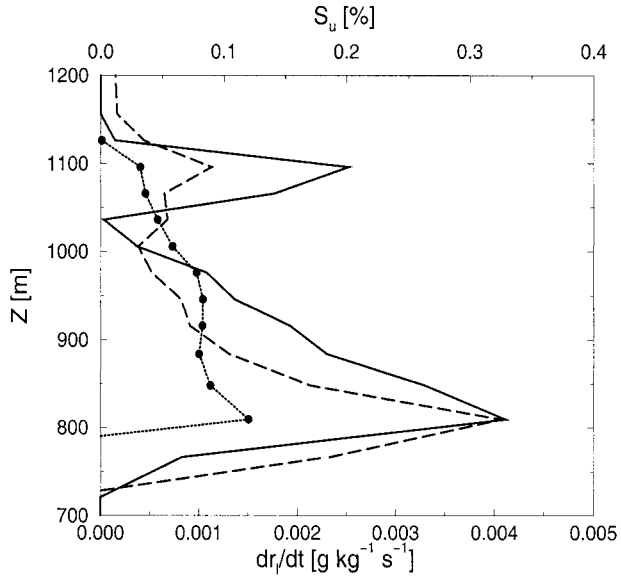

FIG. 16. ERM profiles of the total condensation rate in updrafts (dr_l/dt, solid line) and supersaturation in updrafts (S_u, dashed line) for the no-sedimentation simulation. Included is a profile of S_u from the ensemble TEM simulations (dashed-dotted line). All profiles are averaged over the last 15 min of each simulation.

The ERM solutions suggest that the radiative term is only weakly important as regards drizzle initiation and microphysical evolution in ASC. However, because of the large discrepancies between the TEM results and those of the ERM, future studies will examine why the radiative term produces a weaker overall effect in the ERM by using the above set of possibilities as a guide.

7. Concluding remarks

In this paper, the impacts of radiative heating and cooling on the growth of an explicitly modeled population of drops were considered. The coupling between a radiative transfer model and the explicit microphysical model of Feingold et al. (1994) was done in a consistent fashion. In order to study the radiative impact on drop growth, ERM simulations of ASC were used as a test bed within two modeling frameworks. Since it is difficult to separate the various microphysical–dynamic feedbacks in the ERM, an offline trajectory ensemble model (TEM) was used. The advantages and disadvantages of this approach were discussed in section 3. ERM simulations that included the radiative term were also conducted.

The TEM analysis shows that the radiative effect reduces the time required for the onset of drizzle by up to 30 min in some cases, depending upon the cloud-top residence time of the parcels. This is also shown to depend weakly on the inclusion of SW heating but more strongly on the size of the activated drops. When parcels spend at least 12 min at cloud top, drop spectra develop bimodality, which has been shown to be due to the fact that drops with $r < 10$ μm experience subsaturated conditions and evaporate. Large drops are not necessary for this mechanism to act; in fact, simulations without collection also show this feature. This differential growth characteristic also appears in the ensemble TEM results, with a similar $r \simeq 10$ μm delineation size. The rapid decrease in Q_a for drops with $r < 10$ μm is suggested as the reason for this behavior.

Results using the ensemble TEM calculations show that drizzle production is predominately confined to the large LWC regions near cloud top and that this is strongly increased by including the radiative term. However, plots of drizzle-mass fraction as a function of cloud-top residence time (t_c) show that the radiative term increases drizzle mass in parcels that potentially contribute to drizzle without the radiative effect. In other words, the radiative effect did not produce copious increases in drizzle amounts within parcels that have shorter cloud-top residence times. Of course, parcels with lower t_c values are more numerous, and it therefore seems logical that if drizzle could be produced at smaller t_c, an enhancement in drizzle amounts would occur. Although this did not occur through the radiative term alone, activation of a few large CCN did cause a shift of drizzle production to smaller t_c. In this particular case, it was shown that activation of large CCN was the cause of the shift to smaller t_c, and not the radiative term. Calculations with larger CCN concentrations showed that drizzle suppression was due to the fact that few parcels have long enough cloud-top transects to initiate drizzle production.

The simulations within the ERM framework showed small differences between the cases with the radiative term and those without it. Drizzle onset occurs about 20 min earlier with the radiative term; however, the simulation without the radiative effect quickly caught up and surpassed the control simulation. Model integrations with larger CCN concentrations have shown a similar effect. Simulations without drizzle, and without drizzle and collection, also show a weak impact of the radiative term compared to the TEM results. The reasons for this are not understood at this time, and future work will examine the detailed impact of the radiative term in both ERM and LES frameworks.

Acknowledgments. J. Y. Harrington gratefully acknowledges the support of the Augmentation Awards for Science and Engineering Training under Contract F49620-95-1-0386 and the Geophysical Institute at the University of Alaska Fairbanks. Support for G. Feingold and W. R. Cotton was through the Environmental Sciences Division of the U.S. Department of Energy (under Contract Number DE-FG03-95ER61958) as part of the Atmospheric Radiation Measurement Program, which is part of the DOE Biological and Environmental Research (BER) Program, as well as through the Air Force Office of Scientific Research under Grant F49620-95-1-0132. Discussions with S. M. Kreidenweis were help-

ful. Comments by Phil Austin and one anonymous reviewer substantially improved the content and readability of this paper. The authors are thankful for Brenda Thompson's assistance with the production of this manuscript.

REFERENCES

Ackerman, A. S., O. B. Toon, and P. V. Hobbs, 1995: A model for particle microphysics, turbulent mixing and radiative transfer in the stratocumulus-topped marine boundary layer and comparisons with measurements. *J. Atmos. Sci.*, **52**, 1204–1236.

Austin, P. H., S. Siems, and Y. Wang, 1995: Constraints on droplet growth in radiatively cooled stratocumulus. *J. Geophys. Res.*, **100**, 14 231–14 242.

Barkstrom, B. R., 1978: Some effects of 8–12 μm radiant energy transfer on the mass and heat budgets of cloud droplets. *J. Atmos. Sci.*, **35**, 665–667.

Beard, K. V., 1976: Terminal velocity and shape of cloud precipitation drops aloft. *J. Atmos. Sci.*, **33**, 851–864.

Berry, E. X., and R. L. Reinhardt, 1974: An analysis of cloud drop growth by collection: Part I. Double distributions. *J. Atmos. Sci.*, **31**, 1814–1824.

Bott, A., U. Sievers, and W. Zdunkowski, 1990: A radiation fog model with a detailed treatment of the interaction between radiative transfer and fog microphysics. *J. Atmos. Sci.*, **47**, 2153–2166.

Clark, T. L., 1973: Numerical modeling of the dynamics and microphysics of warm cumulus convection. *J. Atmos. Sci.*, **30**, 857–878.

——, 1974: On modelling nucleation and condensation theory in Eulerian spatial domain. *J. Atmos. Sci.*, **31**, 2099–2117.

Cotton, W. R., and R. A. Anthes, 1989: *Storm and Cloud Dynamics*. Academic Press, 88 pp.

Curry, J. A., 1986: Interactions among turbulence, radiation and microphysics in arctic stratus clouds. *J. Atmos. Sci.*, **43**, 90–106.

Feingold, G., B. Stevens, W. R. Cotton, and R. L. Walko, 1994: An explicit cloud microphysics/LES model designed to simulate the Twomey effect. *Atmos. Res.*, **33**, 207–233.

——, ——, ——, and A. S. Frisch, 1996a: The relationship between drop in-cloud residence time and drizzle production in numerically simulated stratocumulus clouds. *J. Atmos. Sci.*, **53**, 1108–1122.

——, S. M. Kreidenweis, B. Stevens, and W. R. Cotton, 1996b: Numerical simulations of stratocumulus processing of cloud condensation nuclei through collision–coalescence. *J. Geophys. Res.*, **101**, 21 391–21 402.

——, W. R. Cotton, S. M. Kreidenweis, and J. T. Davis, 1999: Impact of giant cloud condensation nuclei on drizzle formation in marine stratocumulus: Implications for cloud radiative properties. *J. Atmos. Sci.*, **56,** 4100–4117.

Fuchs, N. A., 1959: *Evaporation and Droplet Growth in Gaseous Media*. Pergamon Press, 72 pp.

Guzzi, R., and R. Rizzi, 1980: The effect of radiative exchange on the growth of a population of droplets. *Contrib. Atmos. Phys.*, **53**, 351–365.

Hall, W. D., 1980: A detailed microphysical model within a two-dimensional dynamical framework: Model description and preliminary results. *J. Atmos. Sci.*, **37**, 2486–2507.

Harrington, J. Y., 1997: The effects of radiative and microphysical processes on simulated warm and transition season Arctic stratus. Ph.D. dissertation, Colorado State University, 289 pp. [Available from Colorado State University, Dept. of Atmospheric Science, Ft. Collins, CO 80523.]

——, T. Reisin, W. R. Cotton, and S. M. Kreidenweis, 1999: Cloud resolving simulations of Arctic stratus. Part II: Transition-season clouds. *Atmos. Res.*, **51,** 45–75.

Long, A. B., 1974: Solutions to the droplet collection equation for polynomial kernels. *J. Atmos. Sci.*, **31**, 1040–1052.

Olsson, P. Q., J. Y. Harrington, G. Feingold, W. R. Cotton, and S. M. Kreidenweis, 1998: Exploratory cloud resolving simulations of Arctic stratus clouds. Part I: Warm season clouds. *Atmos. Res.*, **47–48**, 573–597.

Pruppacher, H. R., and J. D. Klett, 1997: *Microphysics of Clouds and Precipitation.* Kluwer Academic, 954 pp.

Roach, W. T., 1976: On the effect of radiative exchange on the growth by condensation of a cloud or fog droplet. *Quart. J. Roy. Meteor. Soc.*, **102**, 361–372.

Stephens, G. L., 1983: The influence of radiative transfer on the mass and heat budgets of ice crystals falling in the atmosphere. *J. Atmos. Sci.*, **40**, 1729–1739.

Stevens, B., 1996: On the dynamics of precipitating stratocumulus. Ph.D. dissertation, Colorado State University, 140 pp. [Available from Colorado State University, Dept. of Atmospheric Science, Ft. Collins, CO 80523.]

——, G. Feingold, W. R. Cotton, and R. L. Walko, 1996a: Elements of the microphysical structure of numerically simulated nonprecipitating stratocumulus. *J. Atmos. Sci.*, **53**, 980–1006.

——, ——, R. L. Walko, and W. R. Cotton, 1996b: The spurious production of cloud-edge supersaturations by Eulerian models. *Mon. Wea. Rev.*, **124**, 1034–1041.

——, W. R. Cotton, and G. Feingold, 1998: On a detailed representation of cloud-drop spectra in one- and two-dimensional models of boundary layer clouds: A critique. *Atmos. Res.*, **47–48**, 529–553.

Tsay, S.-C., and K. Jayaweera, 1984: Physical characteristics of Arctic stratus clouds. *J. Climate Appl. Meteor.*, **23**, 584–596.

Tzivion, S., G. Feingold, and Z. Levin, 1987: An efficient numerical solution to the stochastic collection equation. *J. Atmos. Sci.*, **44**, 3139–3149.

——, ——, and ——, 1989: The evolution of raindrop spectra. Part II: Collisional collection/breakup and evaporation in a rainshaft. *J. Atmos. Sci.*, **46**, 3312–3327.

Walko, R. L., W. R. Cotton, M. P. Meyers, and J. Y. Harrington, 1995: New RAMS cloud microphysics parameterization. Part I: The single-moment scheme. *Atmos. Res.*, **38**, 29–62.